Computational Aspects and Numerical Simulations in the Elastic Constants Identification

Elena Ferretti, Antonio Di Leo and Erasmo Viola

DISTART − Department of Structures Transportations Waters Survey and Territory Engineering, University of Bologna, Bologna, Italy

Abstract A numerical code for modeling crack propagation using the Cell Method is proposed. The Leon failure surface is used to compute the direction of crack propagation, and the new crack geometry is realized by an intra-element propagation technique. Automatic remeshing is then activated. Applications in Mode I, Mode II and Mixed Mode are presented to illustrate the robustness of the implementation.

1 Comparison between Discrete and Variational Approach

The use of a discrete formulation instead of a variational one is advantageous, since several problems of the variational formulation are avoided by means of the discrete formulation. With the variational formulation:-

- Field variables $f = f(x, y, z, t)$ are needed, which are point and instant dependent. If not directly in possession of point functions, the variational approach obtains them from the global quantities by means of the density notion and limit process. A subsequent phase of equation discretisation and integration is needed to reach the solution.
- The solution is not obtained for the mesh nodes directly, but extrapolated to them.
- It is not possible to attain convergence greater than the second order.
- Heterogeneities represent an obstacle.
- Singularities of the domain contour represent an obstacle.
- Punctual forces represent an obstacle.
- The definition of a model for treating the zone ahead of the crack edge is needed.

On the contrary, with the discrete formulation:-

- Only global variables $g = g(x, y, z, L, A, V, t)$ are needed, which are point and instant, but also line, area and volume dependent. In a word, global functions are domain and not point functions. Balance equations are expressed using global variables, so they do not contain derivatives and do not therefore require integration.
- The solution is obtained for the mesh nodes directly.
- The convergence order is equal to the FEM one, at worst. One can reache convergences of the fourth order.

- The constitutive matrix can vary from one cell to another, with heterogeneities which can be of the same order than the mesh sides dimension.
- Singularities of the domain contour are no longer an obstacle.
- Punctual forces are no longer an obstacle.
- The definition of a model for treating the zone ahead of the crack edge is no longer needed.

2 Crack Extension Criterion

For finding a crack trajectory, the variational principle of the most common crack theories has been used over the past three decades (Parton and Morozov, 1978). Criteria for the initiation of crack propagation can be obtained on the basis of both energy and force considerations. Historically, at first an energy fracture criterion was proposed by Griffith (1920), then Irwin (1957) formulated a force criterion, while the same time demonstrating the equivalence of the two criteria. The Irwin force criterion for crack extension and the equivalent Griffith energy criterion completely solve the question of the limiting equilibrium state of a cracked continuous elastic body. Nevertheless, there exists a number of other formulations also establishing the limiting equilibrium state of a cracked body. Among these, the best known models are those of Lenov and Panasyuk (1959), Dugdale (1960), Wells (1961), Novozhilov (1969), and McClintock (1958).

Usually, the variational problem of finding the limiting load and the crack propagation direction is reduced to that of finding extreme points of a function of several variables (Parton and Morozov, 1978). In the present paper, the variational approach has been abandoned in favour of a discrete formulation of the crack propagation problem. The discrete formulation used in the following is the Cell Method, said the CM (Tonti, 2001).

When studying crack problems for an elastic-perfectly plastic body with the energy equilibrium criterion, the solution is usually given in the case when the plastic deformation is concentrated in a narrow zone ahead of the crack edge. The thickness of this zone is of the order of elastic displacements. Moreover, when the plastic zone ahead of the edge is thin, the problem is reduced to the solution of an elastic problem instead of an elastic-plastic one. This reduction is based on the fact that, in the linearized formulation, a thin plastic zone may be schematically replaced by an additional cut along the face of which are applied forces replacing the action of the plastically deforming material. Attention is then drawn to the fact that the region of plastic non-linear effects in the model under consideration varies with the external load and represents a plastically deforming material in which the state of stress and strain must be determined from the solution of an elastic-plastic problem. With the discrete formulation, on the contrary, no hypothesis on the shape and dimensions of the plastic zone is needed, and the calculation is performed directly, without having to reduce the problem to an equivalent elastic one. The code for crack trajectory analysis with the CM has been developed by Ferretti (2003)[1].

The crack extension direction and the minimum load required to propagate a crack (limiting load) can be determined by using a variety of criteria:-

[1]The Italian Ministry for Universities and Scientific and Technological Research (MURST) is gratefully acknowledged for its financial support.

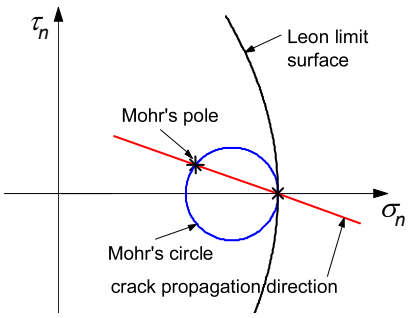

Figure 1. Leon limit surface in the Mohr-Coulomb plane.

- maximal normal stress criterion;
- maximal strain criterion;
- minimum strain energy density fracture criterion;
- maximal strain energy release rate criterion;
- damage law criteria.

In the present paper, the crack extension condition is studied in the Mohr-Coulomb plane. The limiting load is computed as the load satisfying the condition of tangency between the Mohr's circle and the Leon limit surface (Figure 1).

Said c the cohesion, f_c the compressive strength, f_{tb} the tensile strength, τ_n and σ_n, respectively, the shear and normal stress on the attitude of external normal n, the Leon criterion in the Mohr-Coulomb plane is expressed as:

$$\tau_n^2 = \frac{c}{f_c}\left(\frac{f_{tb}}{f_c} + \sigma_n\right). \tag{2.1}$$

The Mohr's circle for the tip neighbourhood is identified by means of the physical significance associated with the CM domain discretization. The CM divides the domain by means of two cell complexes, in such a way that every cell of the first cell complex, which is a simplicial complex, contains one, and one only, node of the other cell complex. In this study, a Delaunay/Voronoi mesh generator is used to generate the two meshes in two-dimensional domains. The primal mesh (the Delaunay mesh) is obtained by subdividing the domain into triangles, so that for each triangle of the triangulation the circumcircle of that triangle is empty of all other sites (Figure 2). The dual mesh (the Voronoi mesh) is formed by the polygons whose vertexes are at the circumcenters of the primal mesh (Figure 2). For each Voronoi site, every point in the region around that site is closer to that site than to any of the other Voronoi sites. The conservation law is enforced on the dual polygon of every primal vertex. To identify the Mohr's circle for the tip neighbourhood, an hexagonal element was inserted at the tip (Ferretti (2003), Figure 2). When the mesh generator is activated, the hexagonal element is divided into equilateral Delaunay triangles and a quasi-regular tip Voronoi cell is generated (the cell

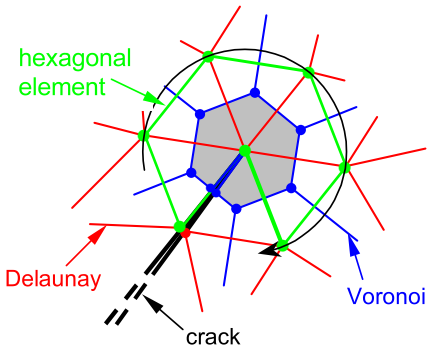

Figure 2. Hexagonal element for analysis in the Mohr-Coulomb plane.

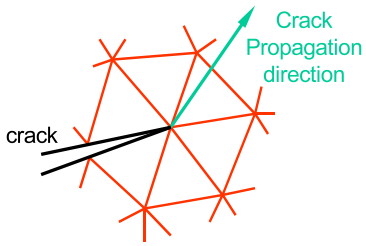

Figure 3. Crack propagation technique.

filled in gray in Figure 2). This allow us to establish a correspondence between the tip stress field and the attitudes corresponding to the sites of the tip Voronoi cell. It has been shown (Ferretti, 2003) that the tension points correctly describe the Mohr's circle in the Mohr-Coulomb plane, for every rotation of the hexagonal element around the tip.

The propagation direction is then derived as the direction of the line joining the tangent point to the Mohr's pole (Figure 1). The crack propagation technique is the nodal relaxation intra-element, with subsequent re-meshing (Figure 3).

3 Constitutive Assumption

The concrete constitutive law here adopted is monotonically non-decreasing, in accordance with the identification procedure for concrete in mono-axial load provided by Ferretti (2001) (Figure 4). It was shown (Ferretti, 2001) how this constitutive law turns out to be size effect insensitive and failure mechanism insensitive for mono-axial compressive load. This result has made it possible to formulate a new concrete law in mono-axial loading, the effective law, which can be considered more representative of the material physical properties than the softening laws are. The tensile branch was here identified

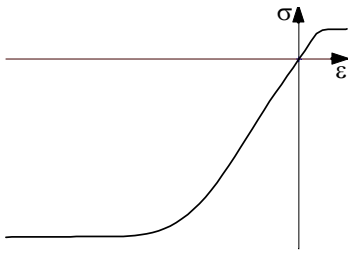

Figure 4. Adopted constitutive law for concrete in mono-axial load.

starting from the compressive one, in the assumption that an homothetic relationship exists between the two branches (Figure 4). A ratio between tensile and compressive strength of 1/12, 1/8, 1/6, 1/4, 1/3 and 1/2 has been considered. The best accordance between analytical and experimental results has been obtained for the ratio equal to 1/8.

4 Numerical Results for Crack Propagation Problems

4.1 Mode I

The code developed by Ferretti (2003) has been extended to provide results in the case of a concrete plate (Figure 5) tensioned at infinity by a load of intensity $p_x = kp_0$ parallel to the $x-$axis, and $p_y = p_0$ parallel to the $y-$axis. The plate has an initial straight crack of length $2l_0$ oriented at an angle α_0 to the $x-$axis (β_0 to the $y-$axis). Numerical results are here provided for various values of k and α_0.

The p_y analysis for $k = 0$ and $\alpha_0 = \pi/4$, plotted on the deformed configuration of a finite area around the crack, is shown in Figure 6 for the initial straight crack. In this Figure, the darker red color corresponds to the maximal tensile stress, while the darker

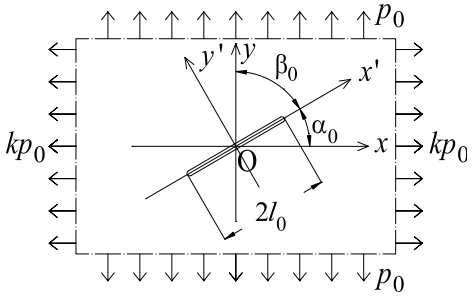

Figure 5. Load and geometrical set-up of the cracked plate.

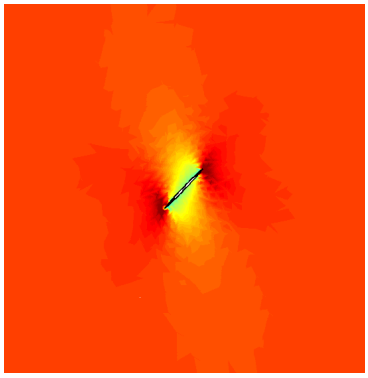

Figure 6. 2D p_y analysis for the initial straight crack with $k = 0$, $\alpha_0 = \pi/4$.

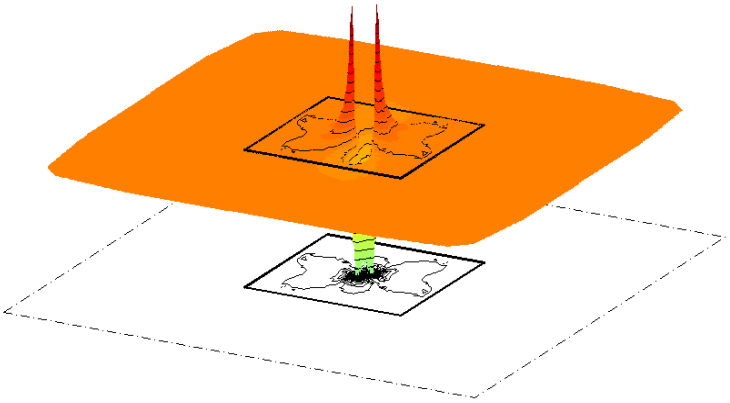

Figure 7. 3D p_y analysis and lines of equal p_y for the initial straight crack with $k = 0$, $\alpha_0 = \pi/4$.

green color corresponds to $p_y = 0$.

In Figure 7, the p_y analysis is performed in 3D, with the level lines plotted in the plane $p_y = 0$. The significance of colors is the same as in Figure 6. The 3D plot correctly shows how p_y reaches a value numerically close to 0 in correspondence with the crack surface. The boxed area in the plane $p_y = 0$ of Figure 7 is the area of Figure 6. As all the level lines are internal to the boxed area, it can be assumed with good approximation that this area represents the stress extinction zone for the initial straight crack.

In Figure 8 and Figure 9, the 2D and 3D p_y analysis for $k = 0$ and $\alpha_0 = \pi/4$ is shown for a generic crack propagation step. The lighter colors of Figures 8 and 9 with respect to those of Figures 6 and 7 are representative of the progressive plate downloading

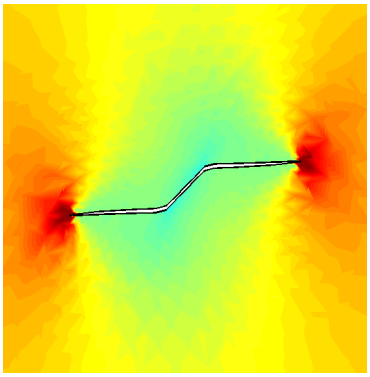

Figure 8. 2D p_y analysis for a generic propagation step with $k = 0$, $\alpha_0 = \pi/4$.

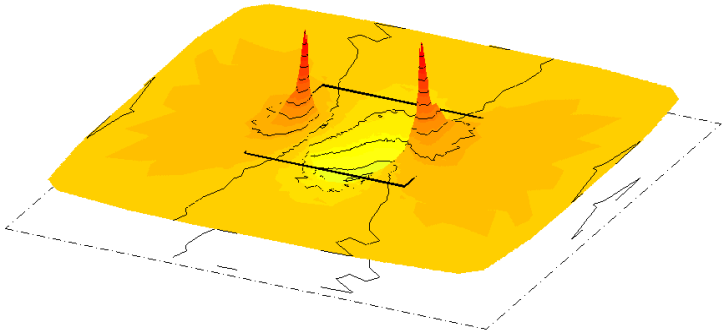

Figure 9. 3D p_y analysis and lines of equal p_y for a generic propagation step with $k = 0$, $\alpha_0 = \pi/4$.

corresponding to a crack propagation. For the same reason, the values in the third axis of Figure 9 are smaller than those of Figure 7. Moreover, in Figure 8 it can be observed how a mono-axial compressive state of stress of small entity (cyan color) arises in the plate, due to the geometrical effect of the non-straight crack deformation in Mode I.

The crack trajectory is plotted in Figure 10 for the value of the angle α_0 equal to $\pi/6$, $\pi/4$ and $\pi/3$, and for the factor k equal to 0, $1/4$, $1/2$, $3/4$ and 1. Also the two meshes of Delaunay-Voronoi were plotted for $k = 0$, in order to show how the adaptive mesh generator recreates the meshes for a generic crack propagation step (Delaunay mesh in red and Voronoi mesh in blue, as indicated in Figure 2). This Figure shows that the crack trajectory tends to approach an asymptote perpendicular to the external tensile load for all the three cases with $k = 0$. The asymptotic behavior is also evident for $k > 0$, but the asymptote is now oriented at an angle γ to the $x-$axis which depends on k:

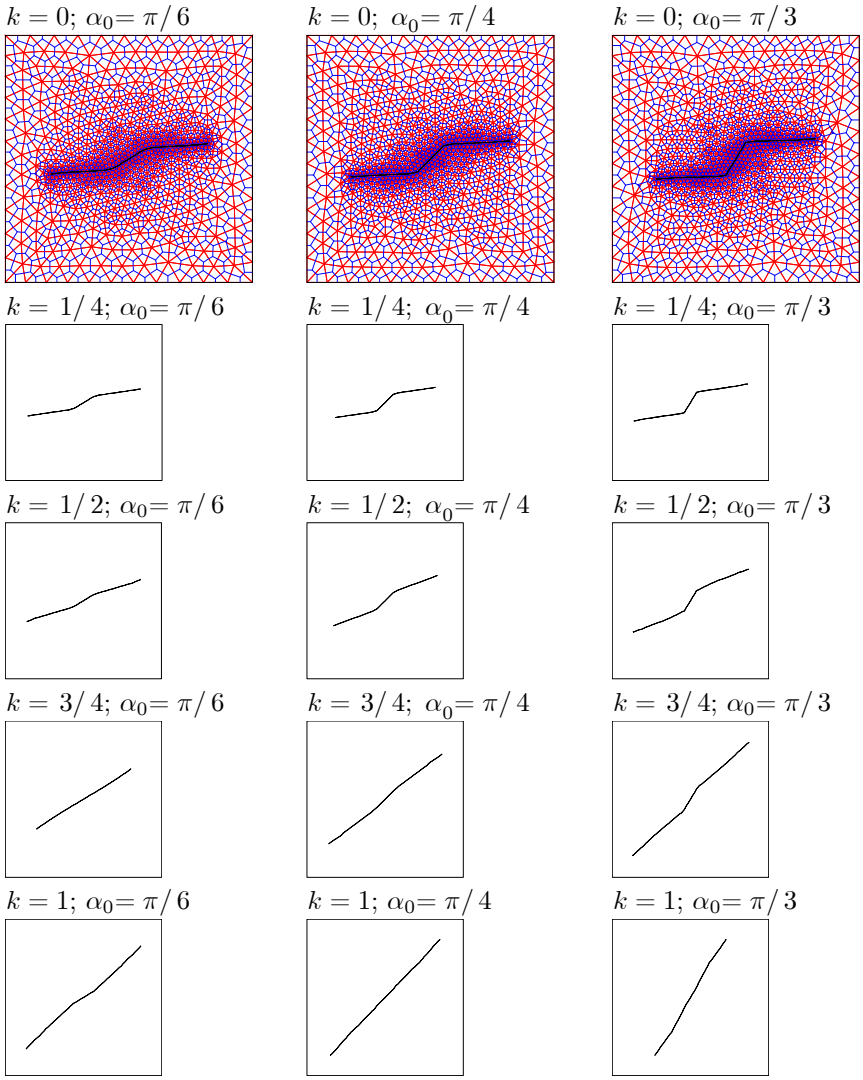

Figure 10. Crack trajectory for $\alpha_0 = \pi/6,\ \pi/4,\ \pi/3$, and $k = 0,\ 1/4,\ 1/2,\ 3/4,\ 1$.

$$\gamma = f(k)\,. \tag{4.1}$$

The angle γ does not depend on the initial inclination α_0, since the crack tends to propagate perpendicularly to the tensile principal direction of the uncracked plate.

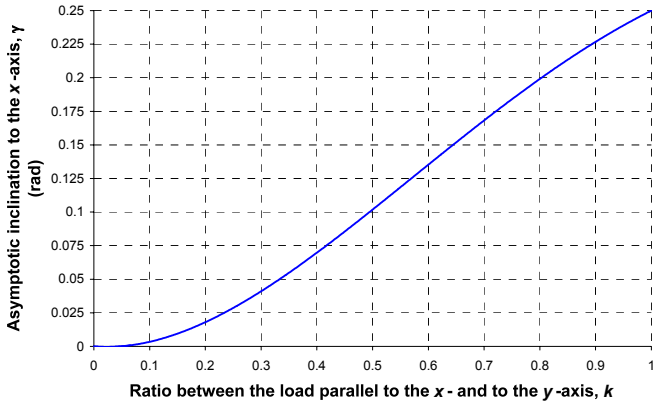

Figure 11. Relation between the angle γ and the ratio k.

For $k = 1$, the angle γ assumes the value $\pi/4$, in good accordance with the homogeneous state of stress represented by this load condition:

$$\gamma|_{k=1} = \frac{\pi}{4}. \tag{4.2}$$

The plot of the function $\gamma = f(k)$ is provided in Figure 11 for the range of values $0 \leq k \leq 1$.

If we know the behavior of the function $\gamma = f(k)$ for $0 \leq k \leq 1$, the behavior of $\gamma = f(k)$ for $1 < k \leq +\infty$ is also known. Actually, the asymptotes of the crack trajectory for a given k and its reciprocal value, $1/k$ (Figure 12), are symmetric with respect to the bisector of the first quadrant in Figure 5, $y = x$. That is to say, the value assumed by γ for a given k is equal to the complementary angle of γ for $1/k$:

$$\gamma\left(\frac{1}{k}\right) = \frac{\pi}{2} - \gamma(k). \tag{4.3}$$

The plot of γ for the complete range of values $0 \leq k \leq +\infty$ can be provided by means of the following change of variable (Figure 13):

$$\psi = 1 - e^{-k}. \tag{4.4}$$

The normalised limiting load in the direction of the $y-$axis, $p_y \Big/ \max_{\alpha_0,k} p_y$, is plotted in Figure 14.a for each value of the angle α_0 ($\beta_0 = 90 - \alpha_0$) and for the factor k equal, respectively, to 0, $1/4$, $1/2$, $3/4$ and 1. This figure exhibits a p_y limiting load increasing with α_0 in the field $0 \leq k < 1$, stating that $\alpha_0 = 0$ is the critical crack orientation angle for all the biaxial load conditions with the $x-$component lower than the $y-$component.

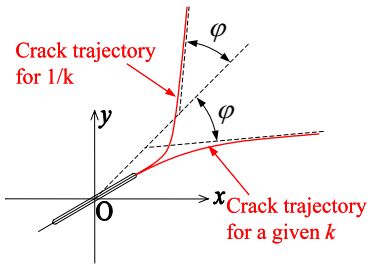

Figure 12. Crack trajectories for a given k and $1/k$.

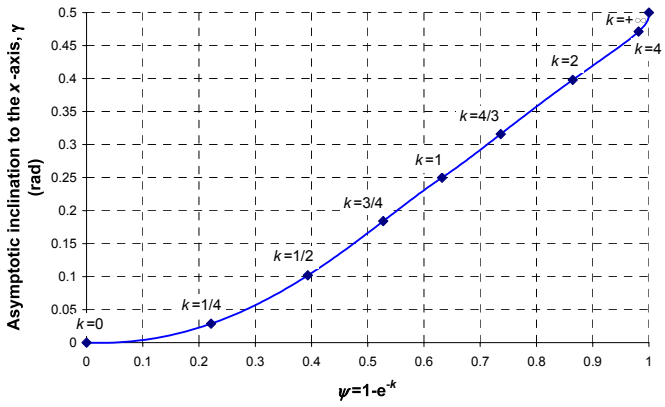

Figure 13. Relation between the angle γ and the variable ψ.

The constant behaviour of the line obtained for $k = 1$ is in good agreement with the homogeneous state of stress represented by this load condition. In this case, all the crack orientations to the $x-$axis return the same limiting load.

The load conditions corresponding to a given k and to its reciprocal, $1/k$, are symmetric with respect to a crack inclination $\alpha_0 = 45°$. In the intent to plot limiting load curves for k and $1/k$ satisfying the symmetry with respect to $\alpha_0 = 45°$, the ideal limiting load p_{id} was defined as:

$$p_{id} = \sqrt{p_x^2 + p_y^2} = p_0\sqrt{k^2 + 1}. \tag{4.5}$$

The limiting load curves in the $\alpha_0 - p_{id} \Big/ \max_{\alpha_0,k} p_{id}$ plane for $0 \leq k \leq +\infty$ are plotted in Figure 14.b. Each line in Figure 14.b represents the function $f_k = p_{id}(\alpha_0)$, returning the value of p_{id} at a given value of k. All the f_k lines together represent the function $f = p_{id}(\alpha_0, k)$, defining the value of the ideal limiting load in function of the crack

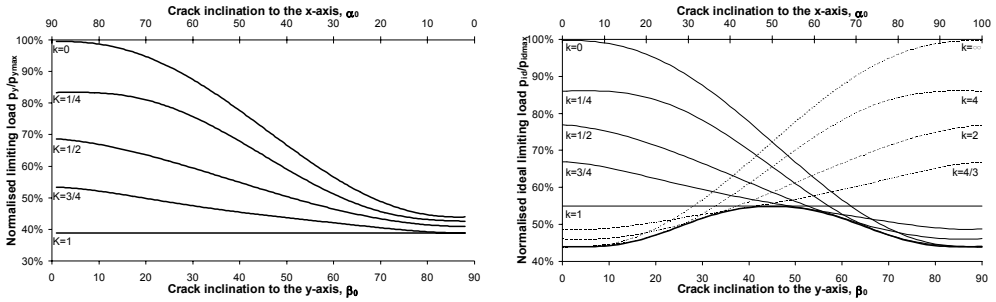

Figure 14. a) Normalised limiting load p_y in function of the crack inclination α_0/β_0 for $0 \leq k \leq 1$; b) Normalised ideal limiting load p_{id} in function of the crack inclination α_0/β_0 for $0 \leq k \leq +\infty$.

orientation and the ratio between the loads in direction of the $x-$ and $y-$axis. The lower envelope of the f_k curves was plotted in thick line in figure Figure 14.b. This line represents the function F defined as:

$$F = F(\alpha_0, k) = \min_{\alpha_0 = const} p_{id}(\alpha_0, k). \tag{4.6}$$

The projection on the $\alpha_0 - k$ plane of the F function, said $\overline{F}$, returns the value of k^{cr} (which is the same, the couple of normalised values p_x^{cr} and p_y^{cr}), corresponding to the minimum value of ideal limiting load p_{id} for a given α_0. In other words, the function $\overline{F}$ can be expressed as the solution of the following differential problem:

$$\overline{F} = k^{cr}(\alpha_0) : \frac{\partial p_{id}(\alpha_0, k)}{\partial k} = 0. \tag{4.7}$$

With the position in Eq. 4.4, it is possible to give a finite 3D representation of p_{id}, in function of α_0 (β_0) and k. Some examples of the 3D surfaces obtained for different values of axis orientation are given in Figure 15. The Figure 15.a is the 3D equivalent representation of the Figure 14.b, while the Figure 15.f is obtained by a 90° rotation of the normalised p_{id} surface around the normalised $p_{id}-$axis. This last plot represents the function $g = p_{id}(k, \alpha_0)$ in the k first independent variable and α_0 second independent variable. The meridians of g give the functions $g_{\alpha_0} = p_{id}(k)$ for a given value of α_0. The lower envelope of the g_{α_0} functions gives the function:

$$G = G(k, \alpha_0) = \min_{k = const} p_{id}(k, \alpha_0). \tag{4.8}$$

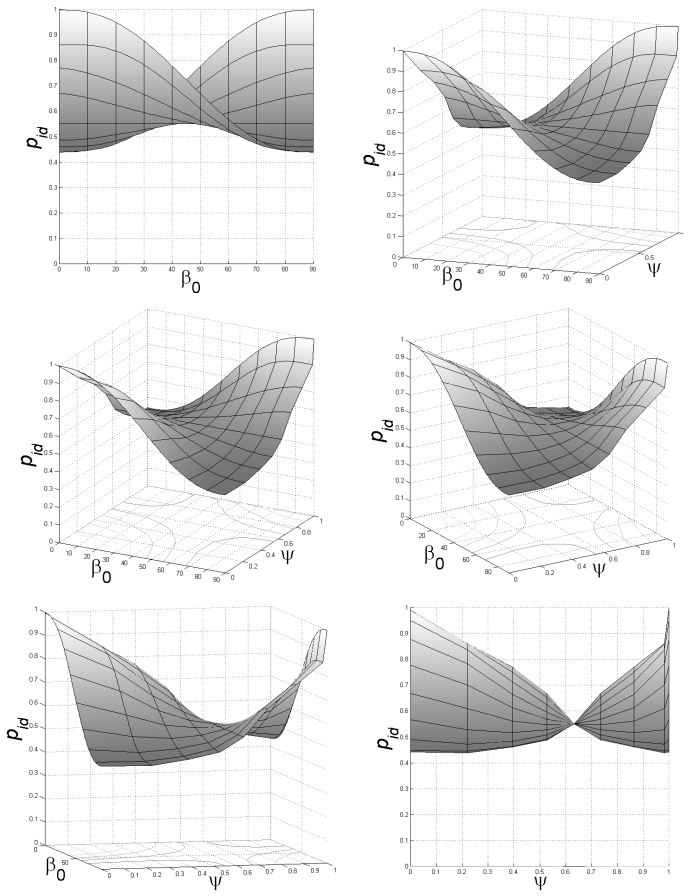

Figure 15. Some examples of finite 3D representation of p_{id}, in function of β_0 and k.

Said $\overline{G}$ the projection on the $k-\alpha_0$ plane of the G function, $\overline{G}$ returns the angle α_0^{cr} minimising p_{id} at a given k. $\overline{G}$ is the solution of the following differential problem:

$$\overline{G} = \alpha_0^{cr}(k) : \frac{\partial p_{id}(\alpha_0, k)}{\partial \alpha_0} = 0. \tag{4.9}$$

As all the g_{α_0} functions intersect for $k = 1$ and they do not have any other point in common, the $\alpha_0 = \alpha_0^{cr}$ minimising p_{id} at a given k results equal to:

$$\alpha_0^{cr} = \begin{cases} 0 & 0 \leq k < 1 \\ [0,\ 90] & k = 1 \\ 90 & 1 < k \leq +\infty \end{cases} \tag{4.10}$$

4.2 Mode II

Results regarding the computation on a geometry of finite dimensions in Mode II are here presented. The computation on finite geometries allows one to avoid the quantitative discrepancy between the experimental results and those calculated via- stress intensity factors (Parton and Morozov, 1978), due to the effect of the specimen boundaries on the stress field around the growing crack. In the case of a beam with two opposite pre-cracks submitted to skew-symmetric load in four-points, the numerical result was so accurate as to allow the complete description of the crack trajectory (Figure 16).

In Figure 16, the darker blue color corresponds to the maximal compressive stress and the darker red color corresponds to the maximal tensile stress.

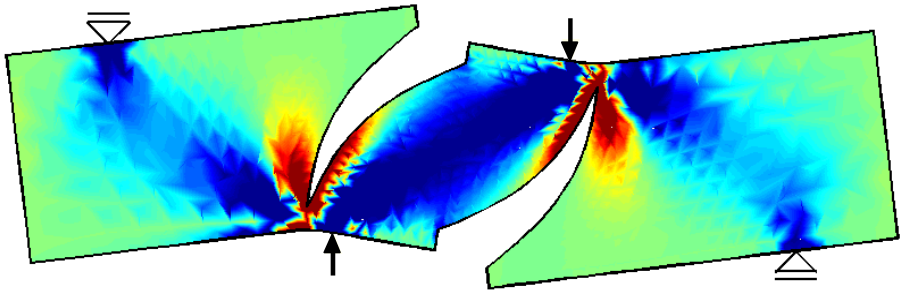

Figure 16. Displacement-stress fields of a beam in skew-symmetric four point bending.

4.3 Mixed Mode

Mixed-Mode crack propagation occurs when the load is applied obliquely to the crack direction and the crack opening direction. If this is the case, the crack can be divided into two parts [Ferretti (2001)]:

part a) Mode I prevails and the two edges of the crack separate;
part b) Mode II prevails and the two edges of the crack slide over one another.

Depending upon the geometry of the domain and the boundary conditions, there may be more than one part a) and more than one part b). Generally speaking, part b) occurs whenever the combination of loading and boundary conditions forces the edges of the crack to close at some point. Numerical simulation is only possible if the position of the point S separating the two parts is known. The dominance of Mode I rather than Mode II crack propagation involves different boundary conditions on the crack surfaces, and it is necessary to specify all the boundary conditions before the simulation starts. In general, S is a function of the load step and crack length, and is, thus, an unknown of the Mixed-Mode problem. To determine S, it is necessary to proceed step-wise.

Numerical results on a concrete compressed cylinder are here presented.

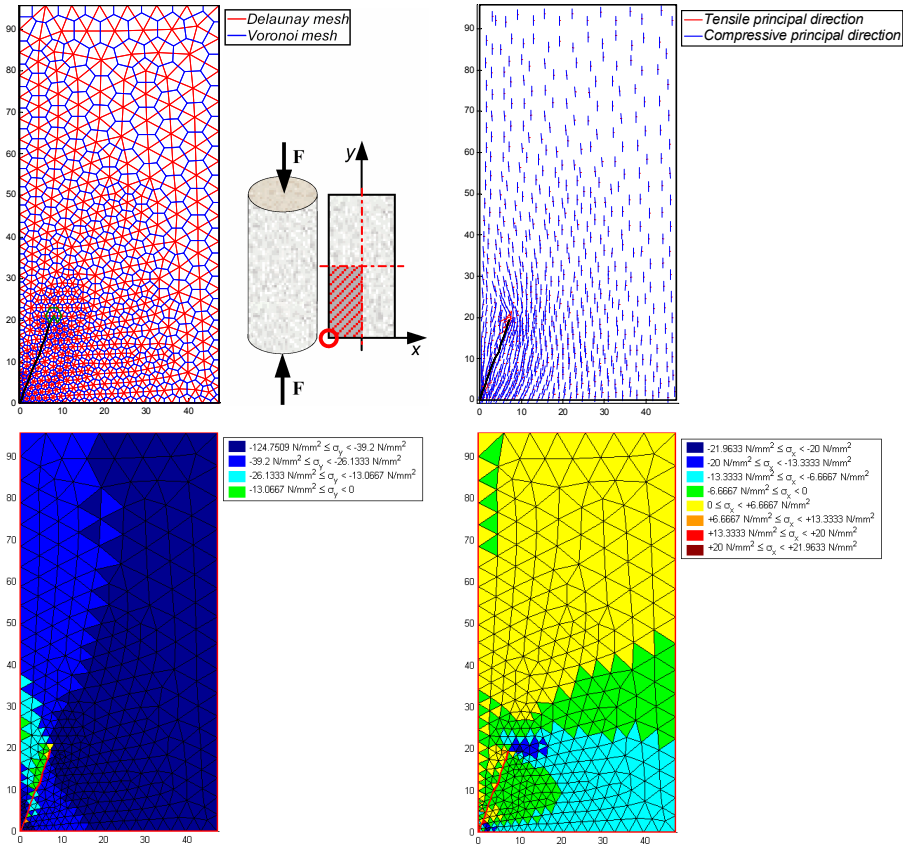

Figure 17. Delaunay and Voronoi discretization of the space domain, computed principal stress directions and stress field in the $y-$ and $x-$axis direction.

5 Conclusions

A crack propagation analysis has been presented for use with the Cell Method, which combines nodal relaxation, intra-element propagation and remeshing. This method permits the mesh dimensions to be refined at specific locations, to improve the solution accuracy. The crack geometry is updated by introducing an extra node at the new crack tip. This is accompanied by a relaxation of the node at the old crack tip.

The crack propagation is studied without using the stress intensity factors and without having to define a model to treat the zone ahead of the crack tip. This allows one to employ the same numerical code for bodies of different dimensions, geometries and boundary

conditions, and for materials of different constitutive laws. As an example of the code versatility in front of the geometrical set-up, the interaction between several cracks oriented at any inclination and propagating in plate of finite/infinite dimensions can be easily investigated. As regards the versatility in front of the constitutive law, the numerical analysis can be performed in the linear or non-linear field, with no adjunctive computational burdens. The stress intensity factors can be estimated a-posteriori, since the code allows us to evaluate the compliance decrement following from a crack propagation.

Both Mode I, Mode II, and Mixed-Mode crack propagation have been considered in this paper. The numerical model incorporates an original approach, which automatically estimates which part of the boundary is subjected to Mode I loading, and which part is subjected to Mode II loading. The numerical model subsequently estimates the size of the relative displacements between nodes on the opposite sides of the crack surface subjected to Mode II loading, allowing sliding contact to be described.

The numerical results show that the CM numerical code can give good predictions for fracture mechanics problems, and validate the CM theory for fracture analysis.

The accuracy of the results indirectly validates the adopted innovative constitutive law for concrete, which turned out to be size effect and failure mechanism insensitive.

Finally, the analysis for finite solids is performed directly, without having to apply corrective factors to the solution on an infinite geometry in the same load conditions.

Bibliography

D.S. Dugdale. Yielding of Steel Sheets Containing Slits. *Journal of the Mechanics and Physics of Solids*, 8(2):100–104, 1960.

E. Ferretti. Crack propagation modeling by remeshing using the Cell Method (CM). *To appear in Computer Modeling in Engineering and Science*, 3:, 2003.

E. Ferretti. Identification of Constitutive Law in Mono-Axially Compressed Damaging Materials. *Advanced in Fracture and Damage Mechanics II. Proc. Int. Conf. on Fracture and Damage Mechanics*, pages 379–384, 2001.

A.A. Griffith. The Phenomena of Rupture and Flow in Solids. *Philosophical Transactions of the Royal Society of London*, Ser. A, 221:163–198, 1920.

G.R. Irwin. Analysis of Stresses and Strains Near the Ends of a Crack Traversing a Plate. *Journal of Applied Mechanics*, 24(3):361–364, 1957.

M.Y. Lenov, V.V. Panasyuk. Development of Minute Cracks in Solids. *Prikladnaya Mekhanika*, 5(4):391–401, 1959.

F. McClintock. Ductile Fracture Instability in Shear. *Journal of Applied Mechanics*, 25: 582–588, 1958.

V.V. Novozhilov. On the Foundations of the Theory of Equilibrium Cracks in Elastic Bodies. *Prikladnaja Matematika i Mekhanika*, 33(5):797–812, 1969.

V.Z. Parton, E.M. Morozov. Elastic-Plastic Fracture Mechanics, MIR Publishers, 1978.

E. Tonti. A Direct Discrete Formulation of Field Laws: the Cell Method. *Computer Modeling in Engineering and Science*, 2(2):237–258, 2001.

A.A. Wells. Unstable Crack Propagation in Metals: Cleavage and Fast Fracture. *Proc. Crack Propagation Symposium*, 1:210–230, 1961.